

Induced current of high temperature superconducting loops by combination of exciting coil and thermal switch

Jia-Wen Wang(王佳雯), Yin-Shun Wang(王银顺), Hua Chai(柴华), Ling-Feng Zhu(祝凌峰), and Wei Pi(皮伟)
Citation: Chin. Phys. B, 2022, 31 (**3**): 037402. DOI: 10.1088/1674-1056/ac1f0a
Journal homepage: http://cpb.iphy.ac.cn; http://iopscience.iop.org/cpb
What follows is a list of articles you may be interested in

Angular dependence of vertical force and torque when magnetic dipole moves vertically above flat high-temperature superconductor

Yong Yang(杨勇), Shuai-Jie Yang(杨帅杰), Wen-Li Yang(杨文莉), and Yun-Yi Wu(吴云翼)
Chin. Phys. B, 2021, 30 (**12**): 127401. DOI: 10.1088/1674-1056/ac0697

Barrier or easy-flow channel: The role of grain boundary acting on vortex motion in type-II superconductors

Yu Liu(刘宇), Xiao-Fan Gou(苟晓凡), and Feng Xue(薛峰)
Chin. Phys. B, 2021, 30 (**9**): 097402. DOI: 10.1088/1674-1056/ac11ea

Lateral magnetic stiffness under different parameters in a high-temperature superconductor levitation system

Yong Yang(杨勇) and Yun-Yi Wu(吴云翼)
Chin. Phys. B, 2021, 30 (**7**): 077404. DOI: 10.1088/1674-1056/abe0c2

Thermal stability and thermoelectric properties of Cd-doped nano-layered Cu_2Se prepared using NaCl flux method

Jianhua Lu(陆建华), Decong Li(李德聪), Wenting Liu(刘文婷), Lanxian Shen(申兰先), Jiali Chen(陈家莉), Wen Ge(葛文), and Shukang Deng(邓书康)
Chin. Phys. B, 2020, 29 (**12**): 127403. DOI: 10.1088/1674-1056/abbbf5

Investigation of dimensionality in superconducting NbN thin film samples with different thicknesses and NbTiN meander nanowire samples by measuring the upper critical field

Mudassar Nazir, Xiaoyan Yang(杨晓燕), Huanfang Tian(田焕芳), Pengtao Song(宋鹏涛), Zhan Wang(王战), Zhongcheng Xiang(相忠诚), Xueyi Guo(郭学仪), Yirong Jin(金贻荣), Lixing You(尤立星), Dongning Zheng(郑东宁)
Chin. Phys. B, 2020, 29 (**8**): 087401. DOI: 10.1088/1674-1056/ab9740

Induced current of high temperature superconducting loops by combination of exciting coil and thermal switch

Jia-Wen Wang(王佳雯), Yin-Shun Wang(王银顺)†, Hua Chai(柴华), Ling-Feng Zhu(祝凌峰), and Wei Pi(皮伟)

State Key Laboratory of New Energy Renewable Power System, North China Electric Power University, Beijing 102206, *China*

(Received 1 July 2021; revised manuscript received 1 July 2021; accepted manuscript online 19 August 2021)

With its commercialization, the second-generation (2G) high temperature superconducting (HTS) RE–Ba–Cu–O (REBCO, RE is rare earth) tape is extensively applied to the superconducting magnets in the high magnetic fields. However, unlike low temperature superconducting (LTS) magnets, the HTS magnet cannot operate in the persistent current mode (PCM) due to the immature superconducting soldering technique. In this paper, an exciting method for two HTS sub-loops, so-called charging and load loops, is proposed by flux pump consisting of exciting coil and controllable thermal switch. Two HTS sub-loops are made of an REBCO tape with two slits. An exciting coil with iron core is located in one sub-loop and is supplied with a triangular waveform current so that magnetic field is generated in another sub-loop. The influence of magnetic flux on induced current in load loop is presented and verified in experiment at 77 K. The relationship between the induced magnetic flux density and the current on the sub-loops having been calibrated, magnetic flux density, and induced current are obtained. The results show that the HTS sub-loops can be excited by a coil with thermal switch and the induced current increases with magnetic flux of exciting coil increasing, which is promising for persistent current operation mode of HTS magnets.

Keywords: bridge, high temperature superconducting (HTS) sub-loops, induced current, thermal switch

PACS: 74.72.–h, 74.78.–w, 84.71.Mn, 85.25.Am **DOI:** 10.1088/1674-1056/ac1f0a

1. Introduction

With the development of its technology and the lowering of cost, the second-generation high temperature superconducting (2G-HTS) RE–Ba–Cu–O (REBCO, RE is rare earth) tape has received wide attention in HTS magnet application.[1] Scientific research institutions have obtained some achievements through continuous exploration in electrical engineering and the superconducting magnets based on 2G HTS tapes.[2–4] The 2G HTS tape has high current carrying capacity, excellent mechanical properties and field performance in high field, it can thus produce strong magnetic fields above 25 T which the low temperature superconducting (LTS) magnets cannot achieve.[5] However, HTS magnet made of 2G HTS tapes still faces many challenges such as twisting, transposing and soldering joint without resistance. The LTS wires can operate in persistent current mode (PCM) in the application of magnets because the technique for soldering the joints without resistance in these superconductors is already well developed.[6–8] According to the standard BS EN ISO 17279-1: 2018, however, soldering technique with the Joint resistance under 10^{-15} Ω becomes bottleneck of the closed-loop operation for HTS magnets.[9] Consequently, the heat-leakage from current leads the operation cost to increase.

To realize PCM of HTS magnet, several HTS magnet models made of 2G HTS tapes have been proposed and excited by flux pump or field cooling in recent years.[10,11] There are several methods of processing HTS magnets in which closed-loop forms without soldering.[12,13] Particularly, an HTS magnet model, stacked by 2G HTS tapes with two slits in the middle of tape, was proposed, and several exciting methods with PCM were preliminary confirmed.[14,15] Each loop of the magnet is independent in carrying the persistent current and any individual loop fault or critical current weak point will not affect the performance of the whole magnet. Therefore, it is significant to study the operation mechanism of magnetic flux in the loops. Note that the charging loop follows the transformer principle that the current on the loop is proportional to $\partial\Phi/\partial t$, and the load loop is only related to the magnetic flux because superconductors obey the law of fluxoid conservation.[16]

This paper aims to realize the influence of magnetic flux on induced current in load loop, which is excited by flux pump consisting of exciting coil and thermal switch. The 2G HTS tape made of an HTS coated conductor is divided into three parts by two slits and stretched out to make jointless persistent current loops. An exciting coil is located in one sub-loop, and a magnetic field is generated in another sub-loop by the flux pump. The thermal switch is located on a bridge between two slits. An experimental setup is established to investigate the induced current of HTS sub-loops under triangular wave magnetization. The excitation principle is further proved by comparing the experimental results with the simulation results. The influence of magnetic flux on induced current in load loop is present and verified in experiment in 77 K. Results show that the HTS sub-loops can be excited by a coil with thermal switch, and the induced current increases with magnetic flux

†Corresponding author. E-mail: yswang@ncepu.edu.cn

© 2022 Chinese Physical Society and IOP Publishing Ltd

of exciting coil increasing, which is promising for persistent current operation mode of HTS magnets.

2. Configuration and principle of flux pump

2.1. Configuration of HTS loops

The loop was made by cutting commercial 2G tapes with a thickness of 0.0681 mm and a width of 12 mm. Figure 1(a) shows the geometrical view of the 2G HTS tape with two slits. Figure 1(b) displays the picture of the tape, which is composed of Hastelloy layer, buffer layer, REBCO film, silver layer and copper layer. Main parameters of the HTS loop are shown in Table 1.

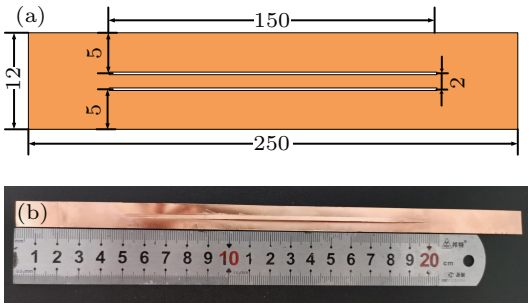


Fig. 1. Schematic diagram of 2G HTS tape with two slits (in units of mm): (a) geometrical view and (b) overview.

Table 1. Thickness of main components of 2G HTS tape.

Thickness	Value
Total (μm)	68.1
Silver layer (μm)	2
Copper layer (μm)	2×7.5
REBCO film (μm)	1
Hastelloy layer (μm)	50
Buffer layer (μm)	100
J_{c0} in self-field and 77 K (MA/cm^2)	3

2.2. Principle of flux pump

The HTS loop can be simplified into two superconducting closed-loops: the closed-loop of the excitation coil, called 'charging loop', and the sub-loop formed in the large circle, named 'load loop'. The common or sharing branch part of the two sub-loops is termed the bridge. The flux pump consists of an applied excitation coil wound by copper wire and a thermal switch located in the bridge as shown in Fig. 2. The excitation coil is located inside the charging loop, and the magnetic field accumulates around load loop.

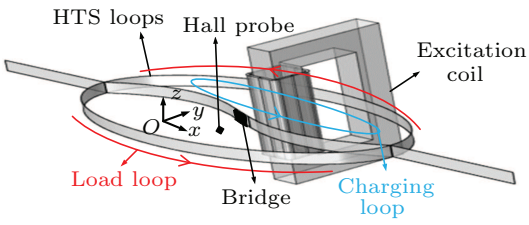


Fig. 2. Principle diagram of flux pump for two HTS sub-loops.

A triangular wave pulse current is generated in the excitation coil of charging loop by a power supply. The thermal switch is realized by a heating resistor on the bridge. Time sequences of both current and temperature of thermal switch are indicated in Fig. 3. Their periods are τ_5–τ_1.

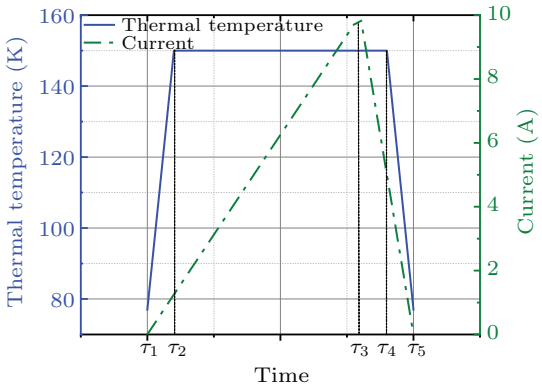


Fig. 3. Time-dependent waveform of current in excitation coil and temperature in thermal switch.

Excitation steps are as follows. 1) The pulse current source in excitation coil turns on at moment τ_1, the flux goes through the loops, and the bridge transfers from superconducting state into normal state gradually which is equivalent to the scenario that the thermal switch is off. 2) The bridge is heated and the resistor is persistent existence at moment τ_2 and extends to τ_4, the thermal switch is thus off within duration of τ_2 to τ_4. The flux in the loop increases till τ_3. 3) The current flows in the HTS loop, in which the pulse current source reaches a maximum at moment τ_3. The resistance of switch starts to decreases at τ_4 and is on again at moment τ_5. 4) Repeat steps 1)–3), the net current increases step by step, that is, the magnetic field accumulates in the load loop.

3. Analysis of magnetic flux generated by induced current of 2G HTS loop

3.1. Excitation process

When a superconducting loop is placed in a changing applied field and the current of the tape is below its critical current, it induces a compensating current inside the loop. Therefore, equation (1) is used to describe the relationship between the change of total magnetic flux inside the ring and the induced current according to Faraday's law,[17,18]

$$-\frac{\mathrm{d}\varphi}{\mathrm{d}t} = L\frac{\mathrm{d}i(t)}{\mathrm{d}t} + V_\mathrm{c}\left(\frac{i(t)}{I_\mathrm{c}}\right)^n, \tag{1}$$

where φ is the total flux, L denotes the inductance, and $i(t)$ refers to the induced current in the loop, $V_\mathrm{c} = E_\mathrm{c}l$, $E_\mathrm{c} = 1 \times 10^{-4}$ V/m is the criterion for defining critical current, $n = 30$ is the power exponent describing the E–J relations, l is the length of the ring, and I_c is the critical current of the loop.

Equation (1) exhibits the relationship between magnetic flux and induced current in the tape. It can be seen that the

magnetic flux is related to the changing rate of the induced current, and a dissipative state emerges which is characterized by an electric field of a resistive nature. When the changing rate is very slow, the heat dissipation inside the sample holder is small. It is observed that the induction of persistent current is directly related to the emergence of a dissipative state. Therefore, the magnetic flux is dominated by the resistive behavior instead of the ramping rate of the applied field, and the temperature inside the loop remains constant.

For even higher maximum current values, magnetic field variations are significant, which reduces the critical current and increases the electric field value in phase with the current. Finally, the induced current achieves the saturated equilibrium when the resistive behavior is almost unchanged.

3.2. Simulation of magnetic flux density

The finite element method (FEM) is used to perform the three-dimensional (3D) simulation of 2G HTS loop, and magnetic field is calculated by the $\boldsymbol{H}$-formula method with the finite element software COMSOL Multiphysics. Magnetic field intensity $\boldsymbol{H}$ is introduced into Maxwell's equations in the $\boldsymbol{H}$-formula.[19,20] The Faraday law of electromagnetic induction and Ampere's law are demonstrated in Eqs. (2) and (3), respectively. Substituting Ohm's law Eq. (3) and magnetic property Eq. (4) into Eqs. (2) and (3), yields Eq. (5).

$$\nabla \times \boldsymbol{E} = -\frac{\partial \boldsymbol{B}}{\partial t}, \tag{2}$$

$$\nabla \times \boldsymbol{H} = \boldsymbol{J}, \tag{3}$$

$$\boldsymbol{E} = \rho \boldsymbol{J}, \tag{4}$$

$$\boldsymbol{B} = \mu_0 \mu_r \boldsymbol{H}, \tag{5}$$

$$\mu_0 \mu_r \frac{\partial \boldsymbol{H}}{\partial t} + \nabla \times (\rho \nabla \times \boldsymbol{H}) = 0, \tag{6}$$

where ρ is the resistivity, μ_0 is the vacuum permeability, and μ_r is the relative permeability.

The solving region consists of the superconducting regions and the air region. An outer boundary surrounding the superconducting and air regions must be defined in order to determine the boundary condition. The outer boundary is far larger than the HTS loop, thus the air region radius is chosen to be 10 times the outer radius. The coordinate system is shown in Fig. 3. The loop is subjected to a background field $f(t)$ along the z direction, and the current is applied to excitation coil in the x direction, which can be imposed on the outer boundary of the model in the forms of Eqs. (6) and (7). The $f(t)$ is the AC magnetic field applied to excitation coil.

$$H_x = H_y = 0, \tag{7}$$

$$H_z = f(t), \tag{8}$$

where H_x, H_y, and H_z are the components of magnetic field intensity in the x, y, z directions respectively.

The electric field characteristic of the HTS loops is expressed by the E–J power law

$$\boldsymbol{E} = E_c \left(\frac{J}{J_c(\boldsymbol{B})} \right)^n, \tag{9}$$

where $J_c(\boldsymbol{B})$ is the critical current density at the magnetic flux density $\boldsymbol{B}$.

The critical current density is related not only to the magnitude of magnetic flux density, but also to its orientation due to its anisotropy, which can be expressed at 77 K by[21]

$$J_c(\boldsymbol{B}) = J_{c0} \left(1 + \frac{1}{B_0} \sqrt{\gamma^{-2} B_{||}^2 + B_\perp^2} \right)^{-\alpha}, \tag{10}$$

where $B_\perp$ and $B_{||}$ are the perpendicular and parallel components of magnetic flux density B to the HTS loops, respectively, J_{c0} is the engineering critical current density in the self-field, $B_0 = 20$ mT is the fitted parameter, $\alpha = 0.65$ is a dimensionless constant, $\gamma = 5$ is a dimensionless fitting parameter.

Two HTS sub-loops use a combination of triangle partitioning and sweeps for finite element meshing. The sweep is used to improve mesh generation, which is suitable for such geometric models with a high aspect ratio. Free triangles are used for meshing in the geometric surface. Figure 4 shows the meshing of HTS sub-loops.

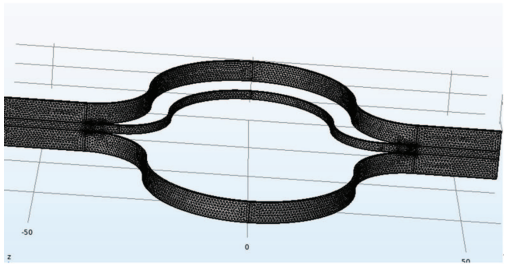


Fig. 4. Meshing of HTS sub-loops using triangle division.

4. Calibration and experiments

4.1. Calibration of induced magnetic flux density and supplied current

In order to obtain the induced current, dependence of magnetic flux density on current needs to be calibrated since

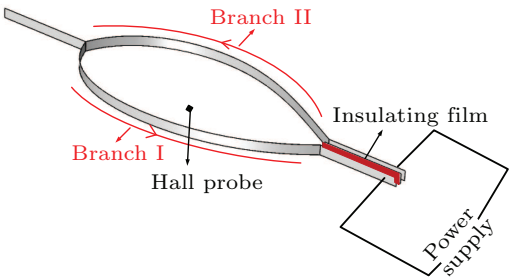


Fig. 5. Experimental arrangement for calibrating relationship between magnetic flux density and supplied current in the loop.

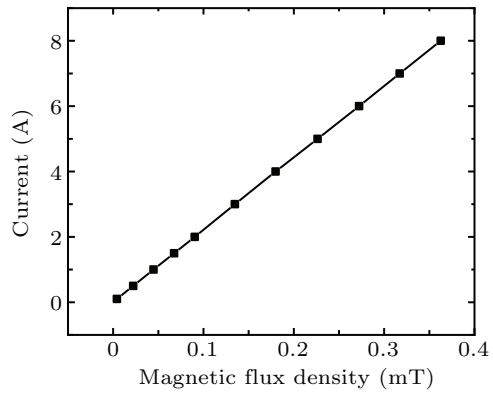


Fig. 6. Calibrated plot of supplied current in the loop against magnetic flux density.

magnetic flux is proportional to current. The experimental arrangement is displayed in Fig. 5, which is the same loop as that in Fig. 2. Firstly, the loop is divided into branch I and branch II, and the terminations are insulated by an insulating film such that the current is directly applied to the loop by a power supply. Then, the loop is fixed by foam, and a hall probe is placed at the same location of the loop as shown in Fig. 2, thus the linear relationship between current and magnetic flux density can be obtained according to the measured induced magnetic flux density values.

Figure 6 shows the linear relationship between supplied current in the loop and induced magnetic flux density in the loop.

4.2. Experiments of induced magnetic flux density

The experimental setup is shown in Fig. 7. The equipment consists of DC power supply (ITECH IT-M3223), voltage supply (Agilent E3631A), and precision multimeter (Keithley 2000), and the assembled experimental setup is shown in Fig. 7, which includes excitation coil, hall probe, thermal switch, and REBCO loop.

The experimental setup is placed in liquid nitrogen, but the equipment is under room temperature. The current source waveform of excitation coil in the flux pump adopts the triangular wave whose rising time is far longer than the transition time. The period is 30 s in the experiment. The rising time of current source is 25 s, the falling time is 5 s. After several pulse periods, the flux accumulates in the center of load loop till the HTS loop reaches saturation.

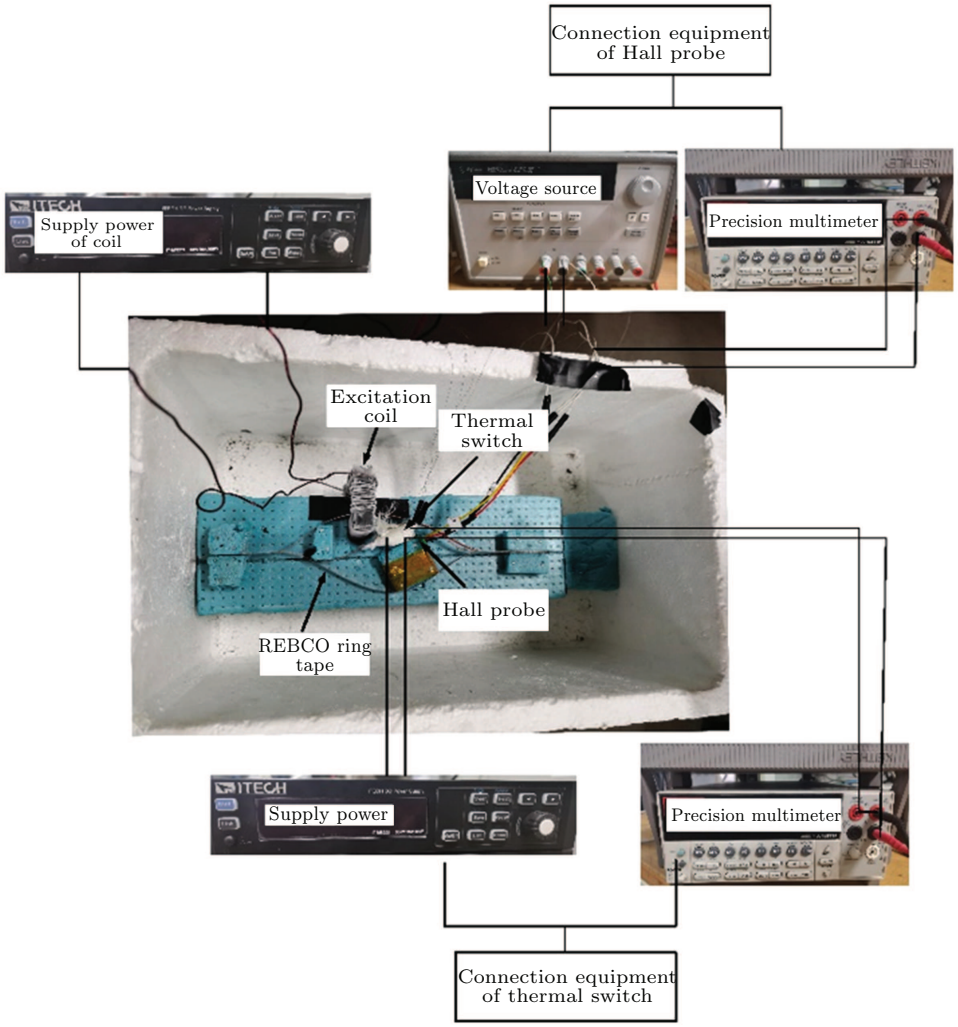


Fig. 7. Equipment and experimental setup in experiment.

5. Results and discussion

According to the principle described in Section 3, the amplitude of the excitation coil is adjusted to 2 A, 4 A, 6 A, 8 A, and 10 A, separately. Figures 8 and 9 show the measured induced current flowing in the load loop. A Hall probe is located in the load loop, which is 10 mm away from the tape as shown in Fig. 2. It can be seen that the saturation induced current depends on excitation current amplitude. The larger the current amplitude, the bigger the saturation induced current is.

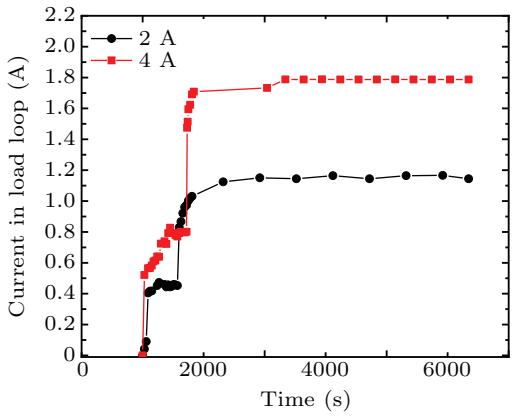


Fig. 8. Time-dependent induced currents in load loop with current amplitudes of 2 A and 4 A, respectively.

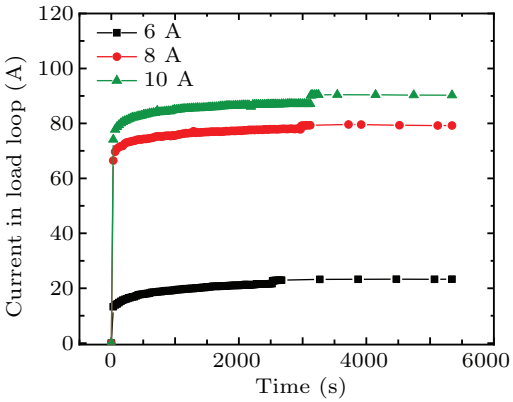


Fig. 9. Time-dependent induced currents in load loop with current amplitudes of 6 A, 8 A, and 10 A, respectively.

The figures show that the induced current increases fast at first, the increasing rate slows down until saturation. The saturation-induced current is related to the current amplitude of the excitation coil. The induced current tends to be saturated at the moment 800 s, 1000 s, 2500 s, 2800 s, and 3000 s when the current amplitude is 2 A, 4 A, 6 A, 8 A, and 10 A, respectively. This phenomenon proves that the magnetic flux of excitation coil turns larger whereas the saturation speed of induced current becomes slower. The final induced currents flowing in the ring are dominated by the resistive behavior of the rings. The maximum load currents are 1.1 A, 1.8 A, 20 A, 78 A, and 90 A in the currents of 2 A, 4 A, 6 A, 8 A, and 10 A respectively.

The simulation results of induced current in z component in the center of load loop are compared with the experimental results, and the accuracy of simulation is verified by the experimental results in Fig. 10. The current amplitude of the excitation coil is 10 A under the control of thermal switch.

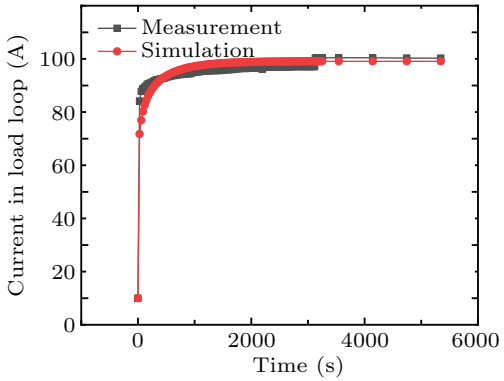


Fig. 10. Comparison of measured current results with simulation results in the center of load loop.

It can be seen that the simulation results are in agreement with the experimental ones. The $\boldsymbol{H}$-formula method is feasible to simulate the HTS sub-loops under thermal switch excited by flux pump.

6. Conclusions

In this work, an HTS loop with two sub-loops is proposed, which is excited by a flux pump with triangular waveform current source and controlled by a thermal switch on the bridge to magnetize the loop without jointing resistance. The influence of magnetic flux on induced current in load loop is verified by numerical simulation and experiment at 77 K, which proves that $\boldsymbol{H}$-formula method is feasible to simulate the HTS sub-loop. The induced current produced by different magnetic fluxes in 2G HTS loop are measured at 77 K. The saturation-induced current of 2G HTS loop increases with the magnetic flux of the excitation coil increasing. The final induced currents flowing in the loop are dominated by the resistive behavior of the loops instead of the ramping rate of the applied field.

The results show that the HTS sub-loops can be excited by flux pump and the induced current increases with the augment of magnetic flux of exciting coil, which, comparing with conventional HTS magnet in PCM, is potential for HTS magnet stacked by many closed-loops operating in PCM without current leads and avoiding soldering bottleneck without resistance.

Acknowledgement

Project supported by the National Natural Science Foundation of China (Grant No. 51977078).

References

[1] Cai C B, Chi C X, Li M J, Liu Z Y, Lu Y M, Guo Y Q, Bai C Y, Lu Q and Dou W Z 2019 *Chin. Sci. Bull.* **64** 827

[2] Yan W H, Cai C B and Zhou D F 2019 *Physics* **48** 733 (in Chinese)

[3] Liu J H, Wang Q L, Qin L, Zhou B Z, Wang K S, Wang Y H, Wang L, Zhang Z L, Dai Y M, Liu H, Hu X N, Wang H, Cui C Y, Wang D G, Wang H, Sun J H, Sun W S and Xiong L 2020 *Supercond. Sci. Technol.* **33** 03

[4] Weijers H W, Markiewicz W D, Gavrilin A V, Voran A J, Viouchkov Y L, Gundlach S R, Noyes P D, Abraimov D V, Bai H Y, Hannahs S T and Murphy T P 2016 *IEEE Trans. Appl. Supercond.* **26** 4300807

[5] Wang Y S 2013 *Fundamental Elements of Applied Superconductivity in Electrical Engineering* (USA) (John Wiley & Sons Pte. Ltd.)

[6] Maeda H and Yanagisawa Y 2014 *IEEE Trans. Appl. Supercond.* **24** 4602412

[7] Noguchi S, Park D, Jiho L, Li Y, Michael P C and Iwasa Y 2019 *IEEE Trans. Appl. Supercond.* **29** 4301005

[8] Yoshikawa M, Yonemura N, Yachida T, Imura T, Shirai Y and Yokoyama S 2016 *IEEE Trans. Appl. Supercond.* **26** 4401105

[9] *Welding. Micro joining of* 2*nd generation high temperature superconductors* (General requirements for the procedure, BS EN ISO 17279-1) (2018)

[10] Lee H G, Kim J G, Lee S W, Kim W S, Lee S W, Choi K D, Hong G W and Ko T K 2006 *Physica C* **445–448** 1099

[11] Yuan X, Wang Y S, Hu Y D, Chen H, Liu M C, Pi W and Cai C B 2018 *IEEE Trans. Appl. Supercond.* **29** 4700405

[12] Yuan X, Wang Y S, Hou Y B, Kan C T and Sun M J 2018 *IEEE Trans. Appl. Supercond.* **28** 4603005

[13] Sheng J, Zhang M, Wang Y W, Li X J, Patel J and Yuan W J 2017 *Supercond. Sci. Technol.* **30** 094002

[14] Qiu D R, Wu W, Pan Y H, Xu S, Zhang Z M, Li Z L, Li Y, Wang Y W, Wang L B, Zhao Y, Zhang Z W, Yang P, Hong Z Y and Jin Z J 2017 *IEEE Trans. Appl. Supercond.* **27** 4601605

[15] Qiu D R, Li Z Y, Wu W, Wang D C, Li X F, Hong Z Y, Ryu K and Jin Z J 2018 *IEEE Trans. Appl. Supercond.* **28** 4601305

[16] Levin G A, Barnes P N, Murphy J, Brunke L and Long J D 2008 *Appl. Phys. Lett.* **93** 062504

[17] Cruz V, Telles G T, Santos B, Ferreira A C and Junior R 2020 *IEEE Trans. Appl. Supercond.* **30** 8200306

[18] Ali M Z, Zheng J X, Huber F, Zhang Z W, Yuan W J and Zhang M 2020 *Supercond. Sci. Technol.* **33** ab794a

[19] Xia J, Bai H Y, Lu J, Andrew V G, Zhou Y H and Weijers H W 2015 *Supercond. Sci. Technol.* **28** 125004

[20] Brambilla R, Grilli F and Martini L 2007 *Supercond. Sci. Technol.* **20** 16

[21] Rostila L, Soderlund L, Mikkonen R and Lehtonen J 2007 *Physica C* **467** 91